Collective dynamics of elastically-coupled myosinV motors

Hailong Lu, Artem K. Efremov, Carol S. Bookwalter, Elena B. Krementsova, Jonathan W. Driver, Kathleen M. Trybus, and Michael R. Diehl

Supporting Information

Figure S1:

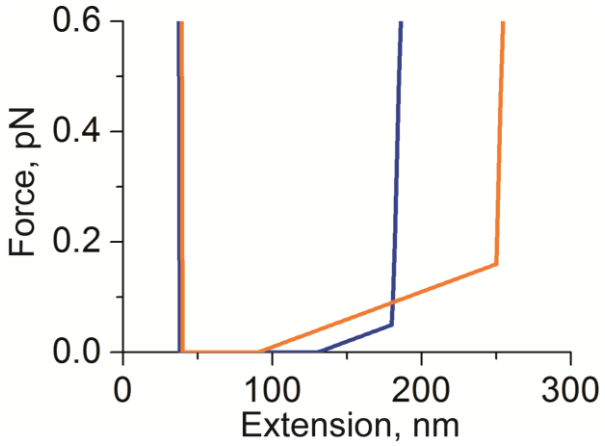

Fig. S1. Force extension curves for 50nm (*blue* curve) and 8 nm (*orange* curve) myosinVa assemblies.

Figure S2:

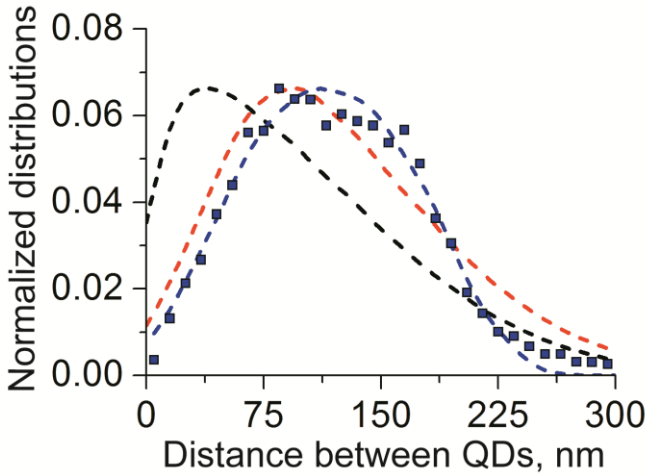

Fig. S2. Theoretical QDs distance distributions obtained from the model: without volume exclusion (*black* curve), with volume exclusion but without the force induced assembly stiffening (*red* curve), and from the model including both of these effects which was used in the rest of the calculations (*blue* curve).

Figure S3:

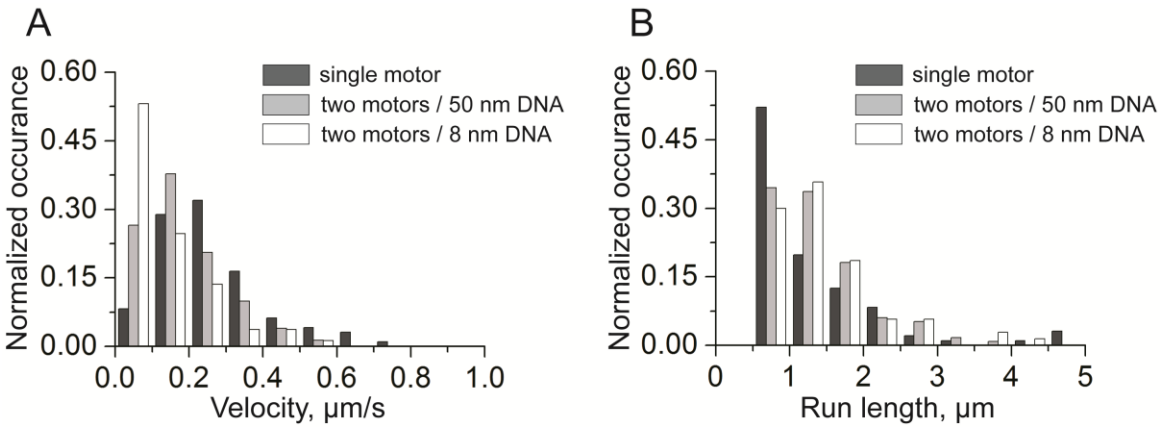

Fig. S3. Experimentally measured velocity and run length distributions of a single myosinVa and 50/8 nm myoVa assemblies.

Figure S4:

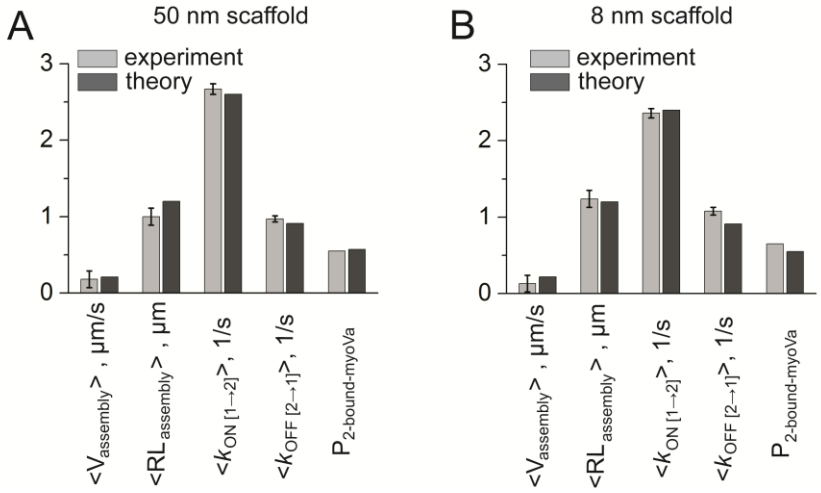

Fig. S4. Transport parameters measured in experiments (*light gray* columns) and predicted by the computational model (*dark gray* columns) for complexes assembled using the 50 nm (A) and 8 nm (B) scaffolds. Error bars indicate standard deviations. V_{single}, $V_{assembly}$, RL_{single} and $RL_{assembly}$ are the average velocities and run lengths of a single myoVa and a two-myoVa complex, respectively. $\langle k_{ON[1\rightarrow 2]} \rangle$ is the average strain-dependent binding rate of diffusing motor during transition from single- to two- bound myosins configuration. $\langle k_{OFF[2\rightarrow 1]} \rangle$ is the average myosin detachment rate during transition from two- to single- bound motor configuration. $P_{2\text{-bound myoVa}}$ is the average probability for the assembly to be in a two actin bound motors state.

Figure S5:

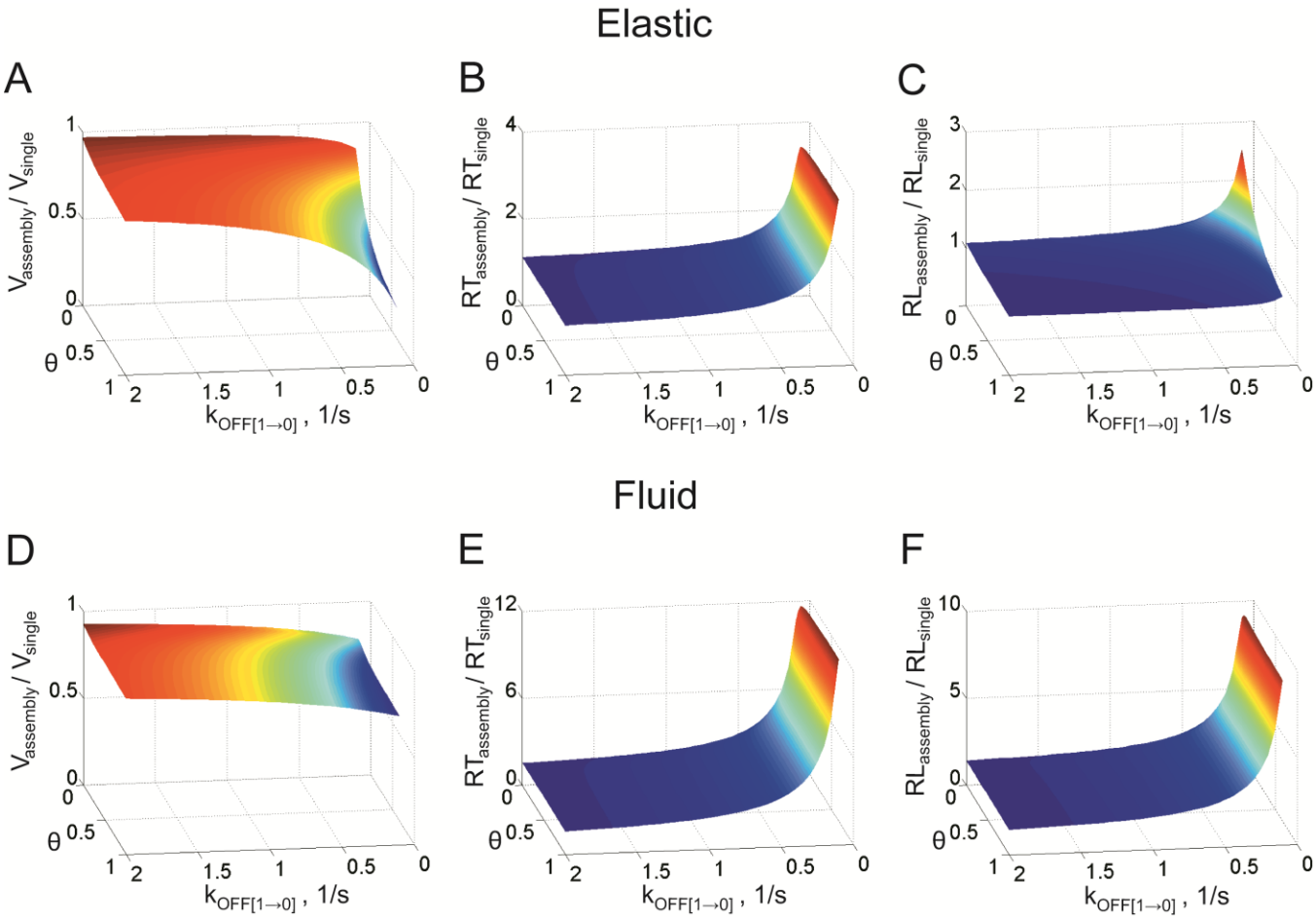

Fig. S5. Two-myosin transport parameters as a function of a single myosin detachment rate $<k_{OFF[1\rightarrow0]}>$and dimensionless factor θ described in the main text. **A-C.** Myosins are elastically coupled. **D-F.** Mysoins have non-elastic coupling between them. $V_{assembly}$, $RT_{assembly}$ and $RL_{assembly}$ are the average velocity, run time and run length of two-myosin system, respectively. V_{single}, RT_{single} and RL_{single} are the average velocity, run time and run length of a single myosin, respectively. The different trends in Panels B and C show that average two-myosin run times and run lengths do not always correlate with each other. When the sensitivity of myosin's stepping rate to strain is varied by adjusting the model parameter θ, as a way to theoretically vary how rapidly motor stepping rates decrease with increasing force, run times do not necessarily change since this parameter does not affect the proportion of times two myosins remain filament bound. However, cargo run lengths do change with increasing θ since the motors step less rapidly. Of note, panels D-F suggest that two-motor velocities are largely unaffected by θ if the motors are not coupled elastically. In this case, two-motor stepping rates are primarily influence by the cargo size-dependent (strain-induced stiffening) effects described in the main text. The weak dependence of $V_{assembly}$, run times, and run lengths on θ reflects the fact that stain / internal forces increase rapidly when the assemblies are stretched beyond a distance equal to a cargo's effective size, but are negligible at small extension distances. Motor stall forces, as opposed to the shape / susceptibility of their *F-V* curves, are more influential in this circumstance.

Supplemental Methods

DNA scaffold construction–Two DNA scaffolds were constructed. For the 8nm double-stranded DNA scaffold, the following 4 ssDNA strands were annealed.

1
GCTTACGCCAGATAGGTCGGTTGCTACACGGACGATGCCACG

2
CGATGTGCCTGCTACGGTGCTGCCAGTGAACTCATTATGCACGCCACGTCCACTAATCGGTATCGCCTATTC
AGGTTCGG

3
GTCACGGACTGAGCGTCGTATGGTAAGCGGCTCGCAATCAGCTCTGACTAGTCTGTAGGTGTCGGATGCCG
AACCTGAATAGGCGATACCG

4
GCTTACGCCAGATAGGTCGGTTCAGTGCCTGACTCGCAGCATACCATTCGCC

For the 50nm double-stranded DNA scaffold, the following 4 ssDNA strands were annealed.
1
CGATGTGCCTGCTACGGTGCTGCCAGTGAACTCATTACGCACGCCACGTCCACTAATCGGTATCGCCTATTC
AGGTTCGGCATCCGACACCTACAGACTCGTCAGAGCTGATTGCGAG

2
GTCACGGACTGAGCGTCGTATGGTAAGCGGCTCGCAATCAGCTCTGACGAGTCTGTAGGTGTCGGATGCCG
AACCTGAATAGGCGATACCGATTAGTGGACGTGGCGTGCGTAATGAGTTCACTGGCA

3
CCGCTTACCATACGACGCTCAGTCCGTGACTTGGCTGGATAGACCGCATTCG

4
GCACCGTAGCAGGCACATCGTTGGCTGGATAGACCGCATTCG

Sequence of the acidic zipper:
LEIEAAALEQENTALETEVAELEQEVQRLENIVSQYRTRYGPL

Sequence of the basic zipper:
LEIEAAALRRRNTALRTRVAELRQRVQRVQRLRNEVSQYETRGPL

Procedure to determine the transformation matrix–A transformation matrix was used to convert the green coordinate into the red coordinate. To construct this matrix, we imaged red and green 0.19μm multicolored fluorescent beads (Ultra Rainbow Particles; Spherotech) that were randomly distributed on a glass cover slip. 50 beads were selected so that they were evenly distributed in the images, and their coordinates in the red and green channels were determined by methods described earlier. The red *xy* coordinates and green *xy* coordinates of the spots were constructed into two 50x2 matrices. The two matrices were then expanded into 50x3 matrices by padding with 1. The red coordinate matrix was divided by the green coordinate matrix to obtain the 3x3 transformation matrix.